THE JOURNAL OF PHYSICAL CHEMISTRY LETTERS
A JOURNAL OF THE AMERICAN CHEMICAL SOCIETY

pubs.acs.org/JPCL

Letter

Hyperfine-Resolved Rotational Spectroscopy of Phenyl Radical

P. Bryan Changala* and Michael C. McCarthy*

Cite This: J. Phys. Chem. Lett. 2023, 14, 5370−5376

Read Online

ACCESS | Metrics & More | Article Recommendations | Supporting Information

ABSTRACT: We present an analysis of the hyperfine-resolved rotational spectrum of gas-phase phenyl radical, c-C_6H_5, between 9 and 35 GHz. The isotropic and anisotropic hyperfine parameters of all five protons and the electronic spin-rotation fine structure parameters are accurately determined from this study, which allow detailed insight into the distribution and interactions of the unpaired electron in this prototypical σ-radical. The implications for laboratory and astronomical investigations of phenyl that are reliant on a precise centimeter-wave catalog are discussed, as are the prospects for detecting and assigning the hyperfine-resolved rotational spectra of other large, weakly polar hydrocarbon chain and ring radicals.

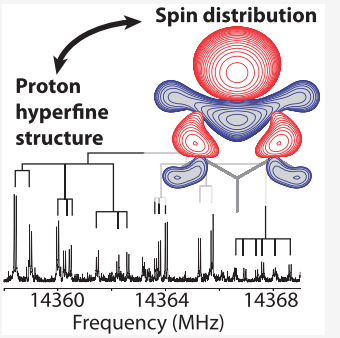

The phenyl radical is a critical intermediate in the formation of large polycyclic aromatic hydrocarbons (PAHs) and soot in combustion, atmospheric, and astronomical environments.[1−8] Its reactivity arises from the unpaired σ electron that results from homolytic cleavage of the strong C−H bond of benzene.[9] The formation of phenyl from smaller radical precursors[10−12] as well as its subsequent ring-addition reactions[1,8,13] can proceed via barrierless, exothermic pathways, highlighting the central role this prototypical σ-type aryl radical plays in low-temperature conditions including those of the interstellar medium.[5] Indeed, the formation of the first aromatic ring is thought to be the rate-limiting step in PAH growth in both interstellar and combustion processes,[6,12] wherein phenyl may represent a more efficient ring-formation route than direct formation of benzene itself.

Previous spectroscopic studies of the phenyl radical have provided considerable insight into its structure and reactivity. Its vibrational and electronic spectra have been measured optically in both cryogenic matrices[14−19] and the gas phase,[20−25] and its critical thermochemical properties have been accurately derived from photoelectron and photoionization measurements.[26−29] Electron spin resonance (ESR) studies in solid- and solution-phase environments[30−33] resolved (albeit at low resolution) the magnetic hyperfine structure arising from the interaction of the unpaired electron spin (S = 1/2) with the nuclear spin of each proton (I_H = 1/2). This extensive hyperfine structure, compounded by additional fine structure due to the interaction of the electron spin with total molecular rotation, however, greatly complicates analysis of its rotational spectrum at very high spectral resolution. Thus, although the pure rotational spectrum of phenyl has been detected in both the microwave and millimeter-wave regions,[34,35] only the latter portion of the spectrum (ca. 150−300 GHz, where proton hyperfine structure has collapsed) has been accurately assigned and fit to date. Using a similar approach, the singly substituted ^{13}C and D isotopic species were measured, yielding a precise molecular structure.[35]

This study revisits the microwave region (9−35 GHz) of phenyl radical. We present a complete assignment of the extensive but well-resolved proton hyperfine structure that is observed via cavity-enhanced Fourier transform microwave (FTMW) spectroscopy. The newly derived spectroscopic parameters provide a direct probe of the spin distribution and spin−orbit interactions of the singly occupied σ orbital in isolated gas-phase phenyl radicals, complementary to prior condensed-phase ESR measurements.[30,32,33] The highly accurate spectroscopic catalog (ca. 1 kHz) resulting from this work enables sensitive and selective detection of phenyl radicals in complex mixtures and reaction environments by narrow- and broadband microwave techniques. The laboratory rest frequencies are also of sufficient accuracy to search for evidence of this fundamental radical in narrow line width interstellar sources such as the cold, dense Taurus Molecular Cloud (TMC-1), the target of the GOTHAM[36] and QUIJOTE[37] radio surveys where many new carbon chains and organic rings have been discovered in the last five years. More generally, our results provide a foundation for the high-resolution analysis and potential radio detection of other large, open-shell, weakly polar hydrocarbons, including benzyl, indenyl, and naphthyl, that are crucial reactive intermediates in astrochemical and combustion processes.

Received: May 8, 2023
Accepted: June 1, 2023
Published: June 6, 2023

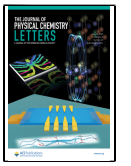

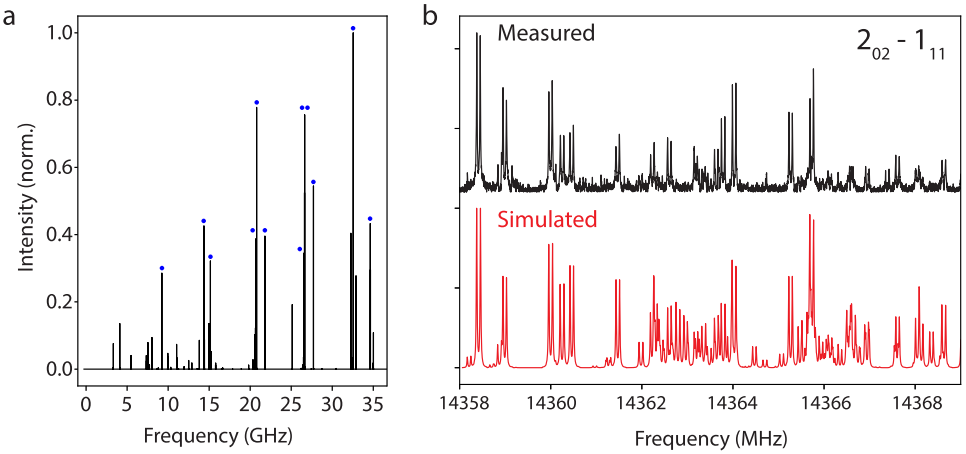

Figure 1. Microwave spectrum of phenyl. (a) Simulated spectrum of the 0−35 GHz region assuming T_{rot} = 2 K. The rotational transitions measured in this study are marked with blue dots. (b) Measured (top, black) and simulated (bottom, red) hyperfine structure of the $2_{02} - 1_{11}$ rotational transition near 14.36 GHz. The measured spectrum is a concatenation of 55 individual spectra, each of which are 0.2 MHz wide; the total integration time is 370 min. The simulated spectrum is derived from the best-fit spectroscopic constants in Tables 1 and 2. The double-peaked line profiles are purely instrumental in origin, arising from the Doppler effect as the gas expands along the axis of the Fabry−Perot cavity. Note that some of the weaker hyperfine components are not observed in the measured spectrum with the expected relative intensity. These $\Delta F = 0$ transitions are very sensitive to magnetic fields, yielding free induction decays with dephasing times comparable to the ring-down time (1−2 μs) of the excitation pulse within the cavity. Because the first ∼10 μs of the FID signal is discarded owing to this residual excitation field, rapidly dephased molecular features are disproportionately attenuated.

Gas-phase phenyl radicals were generated and detected with an upgraded version of the supersonic expansion-discharge source and cavity FTMW spectrometer used for the original microwave measurements.[34,38] A dilute mixture of chlorobenzene in neon buffer gas was supersonically expanded into a large vacuum chamber containing a confocal microwave cavity. As the gas enters the chamber, it passes through two copper ring electrodes held at a 750 V potential, striking an electric discharge that produces phenyl via cleavage of the weak C−Cl bond. Rotational transitions of phenyl were excited by a short pulse of resonant microwave radiation and detected by a sensitive receiver. The rest frequencies of the transitions were measured to an accuracy of 2 kHz. Further details are provided in Experimental Methods.

Twelve pure rotational transitions ($N \leq 5$, $K_a \leq 3$) were measured in the 9−35 GHz frequency range. At high resolution, each transition is a dense collection of features in which several dozen lines are typically clustered within a ∼10 MHz window, the center frequency of which was accurately predicted with the rotational constants derived from the prior mm-wave analysis.[34] Figure 1 provides a comparison between a best-fit simulated spectrum and the measured hyperfine structure for a typical transition ($N_{K_aK_c} = 2_{02} - 1_{11}$).

The assignment and fitting of the spectrum were aided by reliable *a priori* estimates of the fine and hyperfine parameters. A rough estimate of the three nonzero spin-rotation tensor components was derived[39] from the ESR Δg measurements of phenyl in an argon matrix,[32] which yielded ϵ_{aa}, ϵ_{bb}, $\epsilon_{cc} \approx 11 \pm 6$, 0 ± 5, -6 ± 3 MHz. These estimates agree within their measurement uncertainty with high-level *ab initio* predictions[40,41] (ϵ_{aa}, ϵ_{bb}, $\epsilon_{cc} \approx 8.9, 1.5, -5.1 \pm 1.0$ MHz). The nuclear magnetic hyperfine structure is described by an isotropic Fermi contact parameter (a_F) and two independent spin-dipole anisotropic coupling parameters for each proton (T_{cc} and T_{bb-aa}, with $T_{aa} + T_{bb} + T_{cc} = 0$). There are two pairs of symmetry-related protons: one *ortho* pair (located closest to the radical C atom) and one *meta* pair (the next nearest protons). The protons in each pair have equilvalent hyperfine constants, leaving only nine independent hyperfine parameters in total. Matrix and solution-phase ESR measurements[30,32,33] provided relatively accurate experimental values for these hyperfine parameters (1−10% statistical uncertainty, with additional systematic effects from the condensed-phase environment). In addition to theoretical hyperfine estimates available in the literature,[40,41] we performed coupled cluster calculations with the CFOUR package[42,43] including single, double, and perturbative triple valence excitations[44,45] with correlation-consistent triple-ζ basis sets[46] and a restricted open-shell Hartree−Fock reference wavefunction (ROHF-CCSD(T)/cc-pVTZ).

Altogether, the fine and hyperfine interactions split each rotational transition into dozens of individual components that span a few tens of MHz centered around the rotational frequency that would be calculated in the absence of these interactions. Fermi spin-statistics of the protons leads to some simplification of this structure. In the $^2A_1$ ground electronic state of phenyl radical, the total spin of the *ortho* proton pair (I_{ortho} = 0 or 1) and *meta* proton pair (I_{meta} = 0 or 1) can only occur as (I_{ortho}, I_{meta}) = (0, 0) or (1,1) in rotational levels with $K_a + K_c$ = even, and (I_{ortho}, I_{meta}) = (0, 1) or (1,0) with $K_a + K_c$ = odd. These statistics reduce the line density by about a factor of 2 relative to its maximum value. Most of the integrated intensity of a given rotational transition is ultimately carried by between 10 and 25 of the strongest hyperfine components.

Initial assignments were made using spectra simulated with the PGOPHER program.[47] The $\Delta F = +1$ transitions from hyperfine states with the highest possible F values were assigned first based on their relative intensities and qualitative Zeeman splitting patterns under applied bias magnetic fields. After some initial refinement of the spectroscopic constants, additional assignments could then be made with confidence in an iterative, boot-strapped procedure. A total of 185 hyperfine components from 12 rotational transitions were ultimately assigned, and a final least-squares optimization was carried out with the SPFIT

https://doi.org/10.1021/acs.jpclett.3c01243
J. Phys. Chem. Lett. 2023, 14, 5370−5376

program.[48] Tables 1 and 2 summarize the best-fit parameters, which reproduce the measured rest frequencies with an rms residual of 3.6 kHz. The SPFIT input and output files are included in the Supporting Information.

Table 1. Rotation, Centrifugal Distortion, and Spin-Rotation Constants of Phenyl[a]

Parameter	This work	mm-wave[35]
A	6279.17555(12)	6280.203(113)
B	5600.46688(18)	5599.597(92)
C	2959.40030(5)	2959.40114(57)
$D_N \times 10^3$	[1.43716][b]	1.43716(191)
$D_{NK} \times 10^3$	[−2.4335][b]	−2.4335(42)
$D_K \times 10^3$	[1.11047][b]	1.11047(231)
$d_1 \times 10^3$	[0.1182][b]	0.1182
$d_2 \times 10^3$	[0.02909][b]	0.02909
ϵ_{aa}	8.1075(12)	...
ϵ_{bb}	−0.4581(14)	...
ϵ_{cc}	−5.2422(7)	±4.775(18)[c]

[a]All values are in MHz with a 1σ uncertainty given in parentheses. [b]Centrifugal distortion constants in the S-reduced (III^l) representation were held fixed to the values used in the mm-wave analysis of ref 35. [c]Sign of ϵ_{cc} was undetermined and assumed to be positive.[34,35]

Table 2. Hydrogen Hyperfine Parameters of Phenyl[a]

Parameter[b]	This work	ESR (aq)[c]	ESR (Ar)[d]	Calc.[e]
o-a_F	49.3901(242)	48.85(8)	48.8(3)	42.8
o-T_{cc}	−6.5249(19)		−7.0(3)	−6.7
o-T_{bb-aa}	−17.1539(33)		−17.6(3)	−17.5
m-a_F	16.6145(35)	17.52(8)	16.5(3)	13.9
m-T_{cc}	−2.9056(22)		−2.5(3)	−3.0
m-T_{bb-aa}	−1.0140(45)		−0.2(3)	−1.1
p-a_F	5.4113(16)	5.72(8)	5.3(3)	5.1
p-T_{cc}	−1.6612(35)		−2.0(3)	−1.7
p-T_{bb-aa}	1.3678(43)		1.4(3)	0.7

[a]All values are in MHz with a 1σ uncertainty given in parentheses. [b]o = *ortho*, m = *meta*, and p = *para*. [c]Electron spin resonance measurement in aqueous solution.[33] [d]Electron spin resonance measurement in a 4 K argon matrix.[32] [e]Calculated values at the frozen-core ROHF-CCSD(T)/cc-pVTZ level of theory.

The complete set of proton hyperfine parameters determined here allows one to quantify the delocalization of the unpaired radical electron over the σ-bond network of phenyl. Taking the electron density of a H 1s orbital to be $|\psi_{1s}(0)|^2 = 1/\pi$, its atomic isotropic coupling constant is a_F = 1420 MHz. The sum of a_F for the five phenyl hydrogens is 137 MHz, meaning that roughly 10% of the unpaired spin density resides on the H atoms, mostly on the *ortho* pair, which is closest to the cleaved C−H bond. The relative magnitudes of the hydrogen spin densities are well described qualitatively by the singly occupied molecular orbital, illustrated in Figure 2, and the calculated CCSD(T) isotropic and anisotropic hyperfine parameters show excellent agreement with the measured gas-phase values (Table 2). The parameters derived from the microwave data are about 100-fold more precise than previously determined solution- and matrix-phase values,[32,33] but they otherwise do not differ significantly, indicating that the condensed-phase environment effects are small.

The primary contributions to the spin-rotation constants are from second-order spin−orbit interactions.[39] These contributions can be expressed approximately as a sum over both molecular orbitals and atoms

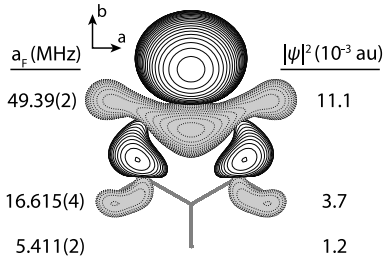

Figure 2. Singly occupied ($11a_1$) molecular orbital of phenyl radical. The ROHF/cc-pVTZ orbital is plotted with an isosurface value of 0.02 au. The experimental isotropic hyperfine parameters (a_F) are shown on the left for the *ortho*, *meta*, and *para* protons, and the derived unpaired spin densities ($|\psi|^2$) are on the right. The a and b principal axes are indicated.

$$\epsilon_{ii} \approx 4B_i \sum_{n\neq 0} \sum_k \zeta_k \frac{\langle n|l_{k,i}|0\rangle\langle 0|l_{k,i}|n\rangle}{E_n - E_0} \quad (1)$$

where B_i is the rotational constant about the ith principal axis, ζ_k is the atomic spin−orbit parameter for carbon atom k (ca. 29 cm^{-1}), $l_{k,i}$ is the electronic orbital angular momentum about axis i and atom k, E_n is the energy of the molecular orbital $|n\rangle$, and $|0\rangle$ is the singly occupied $11a_1$ orbital.[49] The C_{2v} symmetry of phenyl restricts contributions to ϵ_{aa}, ϵ_{bb}, and ϵ_{cc} from excited states of B_1, A_2, and B_2 electronic symmetry, respectively. These symmetry conditions and eq 1 explain the relative magnitudes of the measured spin-rotation constants. Recall that the unpaired electron occupies an a_1 orbital of sp character centered at C_{ipso} (the C atom with the cleaved C−H bond; see Figure 2). The ϵ_{bb} sum involves l_b matrix elements, which are strictly zero for both the C_{ipso} s and p_b atomic orbitals. (The s component has zero total angular momentum, while the p component has a projection of zero along the b symmetry axis.) Moreover, these b-axis interactions couple only to excited states of A_2 symmetry, but a_2 molecular orbitals have zero contribution from C_{ipso} s and p atomic orbitals. The ϵ_{aa} sum will have large positive contributions from interactions induced by l_a, which rotates the C_{ipso} p orbital to overlap closely lying π orbitals. The ϵ_{cc} sum has smaller negative contributions from interactions induced by l_c, which rotates C_{ipso} to overlap b_2 σ bonding orbitals. A relatively crude estimate of these effects can be derived from the Δg estimates of Kasai et al. based on the extended Hückel theory molecular orbitals calculated in their early ESR study of phenyl radical.[32] These results indicate that $\epsilon_{aa} \approx 11$, $\epsilon_{bb} \approx 0$, and $\epsilon_{cc} \approx -4$ MHz, which are in remarkably good agreement with the measured values given the approximations of the calculation. While modern electronic structure methods refine these estimates to $\epsilon_{aa} \approx 8.9 \pm 1$, $\epsilon_{bb} \approx 1.5 \pm 1$, and $\epsilon_{cc} \approx -5.1 \pm 1$ MHz, it appears that a simple, qualitative molecular orbital picture adequately captures the most important physical interactions.

The hyperfine parameters of the ^{13}C nuclei would provide a complete description of the radical electronic structure. Although all four singly substituted ^{13}C isotopologues of phenyl radical have been detected in the mm-wave region,[35] ^{13}C hyperfine structure was evident only in *ipso*-$^{13}CC_5H_5$ (in which the ^{13}C nucleus is located at the nominal radical center and therefore has the largest hyperfine interactions). This species required the inclusion of the isotropic coupling constant

https://doi.org/10.1021/acs.jpclett.3c01243
J. Phys. Chem. Lett. 2023, 14, 5370−5376

$a_F(^{13}C)$, but its gas-phase value could not be determined reliably from the mm-wave spectrum and was instead fixed to the value derived from ESR matrix measurements (a_F = 361(6) MHz[31]). The microwave lines of phenyl are strong enough that single-^{13}C isotopic species may be detectable even in natural abundance. Because their rotational constants (A, B, C) are already accurately known[35] and the spin-rotation constants (ϵ_{aa}, ϵ_{bb}, ϵ_{cc}) satisfy simple isotopic scaling relations,[39] the assignment of their microwave spectra should be relatively straightforward despite the 2−4-fold increase in line density arising from the additional nuclear spin ($I_{^{13}C}$ = 1/2). Determining both the isotropic and anisotropic ^{13}C coupling constants of *ipso*-$^{13}CC_5H_5$ would be particularly illuminating, as it would allow the relative *s* and *p* orbital character of the radical center to be established.

The spectroscopic catalog of phenyl calculated using the best-fit parameters in Tables 1 and 2 has an uncertainty of about 1 kHz for the rest frequencies of the most intense rotational transitions up to 40 GHz. This degree of accuracy enables new spectroscopic applications for investigating the phenyl radical and its chemistry in both the laboratory and in space. Microwave spectroscopy provides sensitive isomer- and isotopologue-specific detection of C_6H_5 in complex reactive mixtures in a frequency range particularly well suited for low-temperature laboratory environments, including cryogenic buffer-gas cooled cells,[50] supersonic expansions,[51] and uniform flows.[52−55]

The astronomical detection of phenyl radical in cold, dense molecular clouds would place a further and likely important constraint on the formation of complex PAHs in the interstellar medium. The well-studied, chemically rich Taurus Molecular Cloud (TMC-1)[56] is the target of two large radio surveys, GOTHAM[36] and QUIJOTE,[37] which cover the 8−36 GHz and 31−50 GHz regions, respectively. These surveys have recently revealed the unexpected presence of several cyclic and aromatic species, including cyanobenzene,[57] cyanonapthalene,[58] indene,[59,60] and cyanoindene,[61] that represent the incipient stages of PAH growth. The chemistry of phenyl is likely critical to the formation of these and even larger PAHs. Its astronomical abundance, or a rigorous upper bound thereof, can now be determined from sensitive radio survey data with high confidence.

The rotational spectra of other large hydrocarbon radicals that are thought to be crucial to PAH growth (e.g., benzyl, indenyl, and naphthyl[6,8]) remain completely unknown. Our results for phenyl suggest that such species may now be amenable to microwave detection and analysis by similar means. The most important factors governing their detectability are molecular size and symmetry (i.e., the rotational partition function, Q_{rot}, and symmetry number, σ), the permanent dipole moment (μ), and the number of proton spins (n_H). Assuming rotational transitions can be optimally polarized, the cavity-FTMW signal scales linearly with μ, and the total figure of merit is proportional to $\mu\sigma/Q_{rot}2^{n_H}$. For astronomical detection, radio emission scales as μ^2, so the relevant figure of merit is $\mu^2\sigma/Q_{rot}2^{n_H}$. Table 3 compares these quantities for several hydrocarbon radicals both smaller and larger in size than phenyl. (We assume rotational temperatures of T_{rot} = 2 K for laboratory supersonic expansions and T_{rot} = 7 K, the typical excitation temperature in TMC-1,[37] for astronomical detection.) These order-of-magnitude estimates illustrate that microwave studies of heavier species with sensitive cavity spectrometers and radio telescopes will be challenging but not insurmountably so. The dipole moments of the resonance-stabilized π-radicals allyl, propargyl, benzyl, and indenyl are particularly small (μ < 0.15 D). As with their closed-shell parents, the much larger dipole moments of the cyano-tagged derivatives of these species (μ = 4−5 D) may make them the preferred targets for both laboratory and astronomical searches.[51,61,62] The propargyl radical is in fact already known both in the laboratory and in TMC-1.[63,64] The microwave detection of the small, moderately polar cyclopropyl radical, *c*-C_3H_5, is particularly favorable by this metric and additionally benefits from the accurate rotational constants derived from existing high-resolution infrared spectroscopy.[65] Indeed, cursory efforts in our laboratory have already been successful in detecting several hyperfine-resolved transitions of *c*-C_3H_5 with a signal-to-noise ratio comparable to phenyl, and a parallel search for its allyl isomer (CH_2CHCH_2) is underway. Detection of still larger hydrocarbon radicals by microwave spectroscopy is an intriguing possibility and would provide another means to critically quantify and assess their roles in gas-phase organic chemistry.

Table 3. Estimated Detectability of Hydrocarbon Radicals by Cavity-FTMW Spectroscopy and Radio Astronomy

	$2^{n_H}/\sigma \times Q_{rot}$ [a]			Figure of merit[c]	
Molecule	2 K	7 K	μ (D)[b]	Lab.	Astro.
phenyl, C_6H_5	7.7×10^2	4.9×10^3	0.87	1.0	1.0
benzyl, C_7H_7	6.0×10^3	3.9×10^4	0.10	0.015	0.0017
indenyl, C_9H_7	1.1×10^4	7.4×10^4	0.14	0.011	0.0017
1-naphthyl, $C_{10}H_7$	3.3×10^4	2.1×10^5	0.87[d]	0.023	0.023
cyclopropyl, *c*-C_3H_5	1.1×10^2	6.4×10^2	0.49	4.1	2.4
allyl, C_3H_5	1.2×10^2	7.3×10^2	0.05	0.38	0.022
propargyl, H_2CCCH	7.2×10^0	3.1×10^1	0.15	18	4.8

[a] Q_{rot} is calculated by direct summation using rigid rotor energies and rotational constants from refs 63 and 65−72. [b] Dipole moments from refs 40, 67, 71, and 73. [c] Figure of merit ($\mu\sigma/Q_{rot}(2\ K)2^{n_H}$ for laboratory cavity detection and $\mu^2\sigma/Q_{rot}(7\ K)2^{n_H}$ for astronomical detection in TMC-1) relative to phenyl. [d] Assumed equal to phenyl.

EXPERIMENTAL METHODS

A dilute mixture of 0.1% chlorobenzene in neon at a total pressure of 2500 Torr was expanded from a solenoid valve in 500 μs pulses at a repetition rate of 5 Hz. As the gas expands into a large vacuum chamber where a confocal microwave cavity is located, the rotational temperature rapidly drops to within a few Kelvin. As the gas exits the valve, it passes through two cylindrical copper ring electrodes which differ in potential by 750 V. At high density, the breakdown voltage is reached, and an electric discharge (20−40 mA peak current) is struck between the electrodes. Phenyl was produced efficiently in the discharge by electron-attachment dissociation of the carbon−halogen bond.[21,22,25] At optimal conditions, the chlorobenzene precursor produced 10−100-fold more phenyl radicals than a benzene precursor.

Rotational transitions of phenyl were excited by a 1 μs pulse of resonant radiation, and the subsequent free induction decay was detected by a sensitive microwave receiver and Fourier transformed. Phenyl has a moderate dipole moment (μ_b = 0.87 D[40]), and its transitions were detected with a signal-to-noise ratio of 140:1 in 400 s of integration in the most favorable cases, noting however that the instantaneous bandwidth is

https://doi.org/10.1021/acs.jpclett.3c01243
J. Phys. Chem. Lett. 2023, 14, 5370−5376

limited to 0.3 MHz because of the high cavity Q. Three mutually orthogonal pairs of Helmholtz coils surrounding the vacuum chamber were tuned to null the magnetic field at the center of the microwave cavity. Zeeman broadening from the residual field at the edges of the cavity volume (<50 mG) prevented the detection of only the weakest and most field-sensitive hyperfine components (i.e., $\Delta F = 0$ transitions, where F is the total spin-rovibronic angular momentum quantum number). The measured rest frequencies have an accuracy of about 2 kHz.

■ ASSOCIATED CONTENT

Supporting Information

The Supporting Information is available free of charge at https://pubs.acs.org/doi/10.1021/acs.jpclett.3c01243.

SPFIT/SPCAT input and output files: `phenyl.lin`, experimental line list; `phenyl.par`, SPFIT parameter input file; `phenyl.fit`, fit results; `phenyl.var`, SPCAT parameter input file; `phenyl.int`, SPCAT dipole input file; `phenyl.cat`, calculated catalog (ZIP)

■ AUTHOR INFORMATION

Corresponding Authors

P. Bryan Changala − *Center for Astrophysics, Harvard & Smithsonian, Cambridge, Massachusetts 02138, United States;* orcid.org/0000-0003-0304-9814; Email: bryan.changala@cfa.harvard.edu

Michael C. McCarthy − *Center for Astrophysics, Harvard & Smithsonian, Cambridge, Massachusetts 02138, United States;* orcid.org/0000-0001-9142-0008; Email: mccarthy@cfa.harvard.edu

Complete contact information is available at: https://pubs.acs.org/10.1021/acs.jpclett.3c01243

Notes

The authors declare no competing financial interest.

■ ACKNOWLEDGMENTS

This work was supported by the U.S. National Science Foundation Award Nos. AST-1908576 and PHY-2110489.

■ REFERENCES

(1) Miller, J. A.; Melius, C. F. Kinetic and thermodynamic issues in the formation of aromatic compounds in flames of aliphatic fuels. *Combust. Flame* **1992**, *91*, 21−39.

(2) Kaiser, R. I.; Asvany, O.; Lee, Y. T.; Bettinger, H. F.; Schleyer, P. v. R.; Schaefer, H. F. Crossed beam reaction of phenyl radicals with unsaturated hydrocarbon molecules. I. Chemical dynamics of phenylmethylacetylene ($C_6H_5CCCH_3$; X^1A') formation from reaction of $C_6H_5(X^2A_1)$ with methylacetylene, $CH_3CCH(X^1A_1)$. *J. Chem. Phys.* **2000**, *112*, 4994−5001.

(3) Golan, A.; Ahmed, M.; Mebel, A. M.; Kaiser, R. I. A VUV photoionization study of the multichannel reaction of phenyl radicals with 1,3-butadiene under combustion relevant conditions. *Phys. Chem. Chem. Phys.* **2013**, *15*, 341−347.

(4) Böhm, H.; Jander, H.; Tanke, D. PAH growth and soot formation in the pyrolysis of acetylene and benzene at high temperatures and pressures: modeling and experiment. *Symp. Int. Combust.* **1998**, *27*, 1605−1612.

(5) Herbst, E. Chemistry in the interstellar medium. *Annu. Rev. Phys. Chem.* **1995**, *46*, 27−54.

(6) Frenklach, M. Reaction mechanism of soot formation in flames. *Phys. Chem. Chem. Phys.* **2002**, *4*, 2028−2037.

(7) Gu, X.; Kaiser, R. I. Reaction dynamics of phenyl radicals in extreme environments: a crossed molecular beam study. *Acc. Chem. Res.* **2009**, *42*, 290−302.

(8) Johansson, K. O.; Head-Gordon, M. P.; Schrader, P. E.; Wilson, K. R.; Michelsen, H. A. Resonance-stabilized hydrocarbon-radical chain reactions may explain soot inception and growth. *Science* **2018**, *361*, 997−1000.

(9) Davico, G. E.; Bierbaum, V. M.; DePuy, C. H.; Ellison, G. B.; Squires, R. R. The C-H bond energy of benzene. *J. Am. Chem. Soc.* **1995**, *117*, 2590−2599.

(10) Zhang, F.; Jones, B.; Maksyutenko, P.; Kaiser, R. I.; Chin, C.; Kislov, V. V.; Mebel, A. M. Formation of the phenyl radical $[C_6H_5(X^2A_1)]$ under single collision conditions: a crossed molecular beam and ab initio study. *J. Am. Chem. Soc.* **2010**, *132*, 2672−2683.

(11) Miller, J. A.; Klippenstein, S. J. The recombination of propargyl radicals and other reactions on a C_6H_6 potential. *J. Phys. Chem. A* **2003**, *107*, 7783−7799.

(12) Zhao, L.; Lu, W.; Ahmed, M.; Zagidullin, M. V.; Azyazov, V. N.; Morozov, A. N.; Mebel, A. M.; Kaiser, R. I. Gas-phase synthesis of benzene via the propargyl radical self-reaction. *Sci. Adv.* **2021**, *7*, 360−381.

(13) Parker, D. S. N.; Zhang, F.; Kim, Y. S.; Kaiser, R. I.; Landera, A.; Kislov, V. V.; Mebel, A. M.; Tielens, A. G. G. M. Low temperature formation of naphthalene and its role in the synthesis of PAHs (polycyclic aromatic hydrocarbons) in the interstellar medium. *Proc. Natl. Acad. Sci. U. S. A.* **2012**, *109*, 53−58.

(14) Pacansky, J.; Bargon, J. Low temperature photochemical studies on acetyl benzoyl peroxide. Observation of methyl and phenyl radicals by matrix isolation infrared spectroscopy. *J. Am. Chem. Soc.* **1975**, *97*, 6896−6897.

(15) Pacansky, J.; Brown, D. W. Photolysis of acetyl benzoyl peroxide isolated in an argon matrix: the stability of the benzoyloxy and acetoxy radicals towards decarboxylation. *J. Phys. Chem.* **1983**, *87*, 1553−1559.

(16) Hatton, W. G.; Hacker, N. P.; Kasai, P. H. The photochemistry of nitrosobenzene: direct observation of the phenyl radical−nitric oxide triplet radical pair in argon at 12 K. *J. Chem. Soc. Chem. Commun.* **1990**, 227−229.

(17) Radziszewski, J. G.; Nimlos, M. R.; Winter, P. R.; Ellison, G. B. Infrared absorption spectroscopy of the phenyl radical. *J. Am. Chem. Soc.* **1996**, *118*, 7400−7401.

(18) Friderichsen, A. V.; Radziszewski, J. G.; Nimlos, M. R.; Winter, P. R.; Dayton, D. C.; David, D. E.; Ellison, G. B. The infrared spectrum of the matrix-isolated phenyl radical. *J. Am. Chem. Soc.* **2001**, *123*, 1977−1988.

(19) Radziszewski, J. Electronic absorption spectrum of phenyl radical. *Chem. Phys. Lett.* **1999**, *301*, 565−570.

(20) Sharp, E. N.; Roberts, M. A.; Nesbitt, D. J. Rotationally resolved infrared spectroscopy of a jet-cooled phenyl radical in the gas phase. *Phys. Chem. Chem. Phys.* **2008**, *10*, 6592−6596.

(21) Buckingham, G. T.; Chang, C.-H.; Nesbitt, D. J. High-resolution rovibrational spectroscopy of jet-cooled phenyl radical: the ν_{19} out-of-phase symmetric CH stretch. *J. Phys. Chem. A* **2013**, *117*, 10047−57.

(22) Chang, C. H.; Nesbitt, D. J. High resolution spectroscopy of jet cooled phenyl radical: The ν_1 and ν_2 a_1 symmetry C−H stretching modes. *J. Chem. Phys.* **2016**, *145*, 044304.

(23) Porter, G.; Ward, B. The electronic spectra of phenyl radicals. *Proc. R. Soc. London A* **1965**, *287*, 457−470.

(24) Tonokura, K.; Norikane, Y.; Koshi, M.; Nakano, Y.; Nakamichi, S.; Goto, M.; Hashimoto, S.; Kawasaki, M.; Sulbaek Andersen, M. P.; Hurley, M. D.; et al. Cavity ring-down study of the visible absorption spectrum of the phenyl radical and kinetics of its reactions with Cl, Br, Cl_2, and O_2. *J. Phys. Chem. A* **2002**, *106*, 5908−5917.

(25) Freel, K.; Park, J.; Lin, M. C.; Heaven, M. C. Cavity ring-down spectroscopy of the phenyl radical in a pulsed discharge supersonic jet expansion. *Chem. Phys. Lett.* **2011**, *507*, 216−220.

(26) Gunion, R. F.; Gilles, M. K.; Polak, M. L.; Lineberger, W. Ultraviolet photoelectron spectroscopy of the phenide, benzyl and phenoxide anions, with ab initio calculations. *Int. J. Mass Spec. Ion Proc.* **1992**, *117*, 601−620.

(27) Ru, B.; Sanov, A. Photoelectron spectra of hot polyatomic ions: a statistical treatment of phenide. *J. Phys. Chem. A* **2022**, *126*, 9423.
(28) Sveum, N. E.; Goncher, S. J.; Neumark, D. M. Determination of absolute photoionization cross sections of the phenyl radical. *Phys. Chem. Chem. Phys.* **2006**, *8*, 592−598.
(29) Stevens, W. R.; Ruscic, B.; Baer, T. Heats of formation of C_6H_5, $C_6H_5^+$, and C_6H_5NO by threshold photoelectron photoion coincidence and active thermochemical tables analysis. *J. Phys. Chem. A* **2010**, *114*, 13134−13145.
(30) Bennett, J. E.; Mile, B.; Thomas, A. The electron spin resonance spectrum of trapped phenyl radicals prepared by chemical reaction at low temperature. *Proc. R. Soc. A* **1966**, *293*, 246−258.
(31) Bennett, J. E.; Mile, B. Electron spin resonance spectra of some σ-type aromatic radicals. *J. Phys. Chem.* **1971**, *75*, 3432−3437.
(32) Kasai, P. H.; Hedaya, E.; Whipple, E. B. Electron spin resonance study of phenyl radicals isolated in an argon matrix at 4 K. *J. Am. Chem. Soc.* **1969**, *91*, 4364−4368.
(33) Zemel, H.; Fessenden, R. W. Electron spin resonance studies of phenyl and pyridyl radicals in aqueous solution. *J. Phys. Chem.* **1975**, *79*, 1419−1427.
(34) McMahon, R. J.; McCarthy, M. C.; Gottlieb, C. A.; Dudek, J. B.; Stanton, J. F.; Thaddeus, P. The radio spectrum of the phenyl radical. *Astrophys. J. Lett.* **2003**, *590*, L61−L64.
(35) Martinez, O.; Crabtree, K. N.; Gottlieb, C. A.; Stanton, J. F.; McCarthy, M. C. An accurate molecular structure of phenyl, the simplest aryl radical. *Angew. Chem.* **2015**, *127*, 1828−1831.
(36) McGuire, B. A.; Burkhardt, A. M.; Loomis, R. A.; Shingledecker, C. N.; Lee, K. L. K.; Charnley, S. B.; Cordiner, M. A.; Herbst, E.; Kalenskii, S.; Momjian, E.; et al. Early science from GOTHAM: project overview, methods, and the detection of interstellar propargyl cyanide ($HCCCH_2CN$) in TMC-1. *Astrophys. J. Lett.* **2020**, *900*, L10.
(37) Cernicharo, J.; Agúndez, M.; Kaiser, R. I.; Cabezas, C.; Tercero, B.; Marcelino, N.; Pardo, J. R.; De Vicente, P. Discovery of benzyne, *o*-C_6H_4, in TMC-1 with the QUIJOTE line survey. *Astron. Astrophys.* **2021**, *652*, L9.
(38) Grabow, J. U.; Palmer, E. S.; McCarthy, M. C.; Thaddeus, P. Supersonic-jet cryogenic-resonator coaxially oriented beam-resonator arrangement Fourier transform microwave spectrometer. *Rev. Sci. Instrum.* **2005**, *76*, 093106.
(39) Curl, R. F. The relationship between electron spin rotation coupling constants and *g*-tensor components. *Mol. Phys.* **1965**, *9*, 585−597.
(40) Barone, V.; Biczysko, M.; Bloino, J.; Egidi, F.; Puzzarini, C. Accurate structure, thermodynamics, and spectroscopy of medium-sized radicals by hybrid coupled cluster/density functional theory approaches: The case of phenyl radical. *J. Chem. Phys.* **2013**, *138*, 234303.
(41) Mattar, S. M. Accurate calculation of the phenyl radical's magnetic inequivalency, relative orientations of its spin hamiltonian tensors, and its electronic spectrum. *J. Phys. Chem. A* **2007**, *111*, 251−260.
(42) Matthews, D. A.; Cheng, L.; Harding, M. E.; Lipparini, F.; Stopkowicz, S.; Jagau, T.-C.; Szalay, P. G.; Gauss, J.; Stanton, J. F. Coupled-cluster techniques for computational chemistry: The CFOUR program package. *J. Chem. Phys.* **2020**, *152*, 214108.
(43) Stanton, J. F.; Gauss, J.; Cheng, L.; Harding, M. E.; Matthews, D. A.; Szalay, P. G. CFOUR, Coupled-Cluster techniques for Computational Chemistry, a quantum-chemical program package. With contributions from A. Asthana, A.A. Auer, R.J. Bartlett, U. Benedikt, C. Berger, D.E. Bernholdt, S. Blaschke, Y. J. Bomble, S. Burger, O. Christiansen, D. Datta, F. Engel, R. Faber, J. Greiner, M. Heckert, O. Heun, M. Hilgenberg, C. Huber, T.-C. Jagau, D. Jonsson, J. Jusélius, T. Kirsch, M.-P. Kitsaras, K. Klein, G.M. Kopper, W.J. Lauderdale, F. Lipparini, J. Liu, T. Metzroth, L.A. Mück, D.P. O'Neill, T. Nottoli, J. Oswald, D.R. Price, E. Prochnow, C. Puzzarini, K. Ruud, F. Schiffmann, W. Schwalbach, C. Simmons, S. Stopkowicz, A. Tajti, J. Vázquez, F. Wang, J.D. Watts, C. Zhang, X. Zheng, and the integral packages MOLECULE (J. Almlöf and P.R. Taylor), PROPS (P.R. Taylor), ABACUS (T. Helgaker, H.J. Aa. Jensen, P. Jørgensen, and J. Olsen), and ECP routines by A. V. Mitin and C. van Wüllen. For the current version, see http://www.cfour.de.
(44) Gauss, J.; Lauderdale, W. J.; Stanton, J. F.; Watts, J. D.; Bartlett, R. J. Analytic energy gradients for open-shell coupled-cluster singles and doubles (CCSD) calculations using restricted open-shell Hartree—Fock (ROHF) reference functions. *Chem. Phys. Lett.* **1991**, *182*, 207.
(45) Watts, J. D.; Gauss, J.; Bartlett, R. J. Coupled-cluster methods with noniterative triple excitations for restricted open-shell Hartree−Fock and other general single determinant reference functions. Energies and analytical gradients. *J. Chem. Phys.* **1993**, *98*, 8718.
(46) Dunning, T. H. Gaussian basis sets for use in correlated molecular calculations. I. The atoms boron through neon and hydrogen. *J. Chem. Phys.* **1989**, *90*, 1007.
(47) Western, C. M. *PGOPHER*, ver 10.1; University of Bristol Research Data Repository, 2018; DOI: 10.5523/bris.3mqfb4glgkr8a2rev7f73t300c.
(48) Pickett, H. M. The fitting and prediction of vibration-rotation spectra with spin interactions. *J. Mol. Spectrosc.* **1991**, *148*, 371−377.
(49) Stone, A. J. Gauge invariance of the g tensor. *Proc. R. Soc. A* **1963**, *271*, 424−434.
(50) Porterfield, J. P.; Satterthwaite, L.; Eibenberger, S.; Patterson, D.; McCarthy, M. C. High sensitivity microwave spectroscopy in a cryogenic buffer gas cell. *Rev. Sci. Instrum.* **2019**, *90*, 053104.
(51) McCarthy, M. C.; Lee, K. L. K.; Carroll, P. B.; Porterfield, J. P.; Changala, P. B.; Thorpe, J. H.; Stanton, J. F. Exhaustive product analysis of three benzene discharges by microwave spectroscopy. *J. Phys. Chem. A* **2020**, *124*, 5170−5181.
(52) Oldham, J. M.; Abeysekera, C.; Joalland, B.; Zack, L. N.; Prozument, K.; Sims, I. R.; Park, G. B.; Field, R. W.; Suits, A. G. A chirped-pulse Fourier-transform microwave/pulsed uniform flow spectrometer. I. The low-temperature flow system. *J. Chem. Phys.* **2014**, *141*, 154202.
(53) Abeysekera, C.; Zack, L. N.; Park, G. B.; Joalland, B.; Oldham, J. M.; Prozument, K.; Ariyasingha, N. M.; Sims, I. R.; Field, R. W.; Suits, A. G. A chirped-pulse Fourier-transform microwave/pulsed uniform flow spectrometer. II. Performance and applications for reaction dynamics. *J. Chem. Phys.* **2014**, *141*, 214203.
(54) Gurusinghe, R. M.; Dias, N.; Krueger, R.; Suits, A. G. Uniform supersonic flow sampling for detection by chirped-pulse rotational spectroscopy. *J. Chem. Phys.* **2022**, *156*, 014202.
(55) Hearne, T. S.; Abdelkader Khedaoui, O.; Hays, B. M.; Guillaume, T.; Sims, I. R. A novel Ka-band chirped-pulse spectrometer used in the determination of pressure broadening coefficients of astrochemical molecules. *J. Chem. Phys.* **2020**, *153*, 084201.
(56) Gratier, P.; Majumdar, L.; Ohishi, M.; Roueff, E.; Loison, J. C.; Hickson, K. M.; Wakelam, V. A new reference chemical composition for TMC-1. *Astrophys. J. Suppl. Ser.* **2016**, *225*, 25.
(57) McGuire, B. A.; Burkhardt, A. M.; Kalenskii, S.; Shingledecker, C. N.; Remijan, A. J.; Herbst, E.; McCarthy, M. C. Detection of the aromatic molecule benzonitrile (c-C_6H_5CN) in the interstellar medium. *Science* **2018**, *359*, 202−205.
(58) McGuire, B. A.; Loomis, R. A.; Burkhardt, A. M.; Lee, K. L. K.; Shingledecker, C. N.; Charnley, S. B.; Cooke, I. R.; Cordiner, M. A.; Herbst, E.; Kalenskii, S.; et al. Detection of two interstellar polycyclic aromatic hydrocarbons via spectral matched filtering. *Science* **2021**, *371*, 1265−1269.
(59) Burkhardt, A. M.; Lee, K. L. K.; Changala, P. B.; Shingledecker, C. N.; Cooke, I. R.; Loomis, R. A.; Wei, H.; Charnley, S. B.; Herbst, E.; McCarthy, M. C.; et al. Discovery of the pure polycyclic aromatic hydrocarbon indene (*c*-C_9H_8) with GOTHAM observations of TMC-1. *Astrophys. J. Lett.* **2021**, *913*, L18.
(60) Cernicharo, J.; Agúndez, M.; Cabezas, C.; Tercero, B.; Marcelino, N.; Pardo, J. R.; De Vicente, P. Pure hydrocarbon cycles in TMC-1: Discovery of ethynyl cyclopropenylidene, cyclopentadiene, and indene. *Astron. Astrophys.* **2021**, *649*, L15.
(61) Sita, M. L.; Changala, P. B.; Xue, C.; Burkhardt, A. M.; Shingledecker, C. N.; Lee, K. L. K.; Loomis, R. A.; Momjian, E.; Siebert, M. A.; Gupta, D.; et al. Discovery of interstellar 2-cyanoindene (2-

C_9H_7CN) in GOTHAM observations of TMC-1. *Astrophys. J. Lett.* **2022**, *938*, L12.
(62) Cernicharo, J.; Fuentetaja, R.; Cabezas, C.; Agúndez, M.; Marcelino, N.; Tercero, B.; Pardo, J. R.; de Vicente, P. Discovery of five cyano derivatives of propene with the QUIJOTE line survey. *Astron. Astrophys.* **2022**, *663*, L5.
(63) Tanaka, K.; Sumiyoshi, Y.; Ohshima, Y.; Endo, Y.; Kawaguchi, K. Pulsed discharge nozzle Fourier transform microwave spectroscopy of the propargyl radical (H_2CCCH). *J. Chem. Phys.* **1997**, *107*, 2728−2733.
(64) Agúndez, M.; Cabezas, C.; Tercero, B.; Marcelino, N.; Gallego, J. D.; de Vicente, P.; Cernicharo, J. Discovery of the propargyl radical (CH_2CCH) in TMC-1: One of the most abundant radicals ever found and a key species for cyclization to benzene in cold dark clouds. *Astron. Astrophys.* **2021**, *647*, L10.
(65) Dong, F.; Davis, S.; Nesbitt, D. J. Slit discharge IR spectroscopy of a jet-cooled cyclopropyl radical: structure and intramolecular tunneling dynamics. *J. Phys. Chem. A* **2006**, *110*, 3059−3070.
(66) Kortyna, A.; Samin, A. J.; Miller, T. A.; Nesbitt, D. J. Sub-Doppler infrared spectroscopy of resonance-stabilized hydrocarbon intermediates: ν_3/ν_4 CH stretch modes and CH_2 internal rotor dynamics of benzyl radical. *Phys. Chem. Chem. Phys.* **2017**, *19*, 29812−29821.
(67) NIST Computational Chemistry Comparison and Benchmark Database NIST Standard Reference Database Number 101 Release 22, May 2022; Johnson, R. D., III; http://cccbdb.nist.gov/; DOI: 10.18434/T47C7Z.
(68) Uy, D.; Davis, S.; Nesbitt, D. J. High-resolution infrared spectroscopy of jet-cooled allyl radical (CH_2CHCH_2): in-phase (ν_1) and out-of-phase (ν_{13}) antisymmetric CH_2 stretching vibrations. *J. Chem. Phys.* **1998**, *109*, 7793−7802.
(69) Han, J.-X.; Utkin, Y. G.; Chen, H.-B.; Hunt, N. T.; Curl, R. F. High-resolution infrared spectra of jet-cooled allyl radical (CH_2CHCH_2): ν_2, ν_3 and ν_{14} C−H stretch vibrations. *J. Chem. Phys.* **2002**, *116*, 6505−6512.
(70) DeSain, J. D.; Thompson, R. I.; Sharma, S. D.; Curl, R. F. The rotationally resolved infrared spectrum of the ν_1 stretch of the allyl radical. *J. Chem. Phys.* **1998**, *109*, 7803−7809.
(71) The rotational constants and dipole moment of indenyl were estimated by their CCSD(T)/cc-pVTZ equilibrium values calculated in this work.
(72) Ervin, K. M.; Ramond, T. M.; Davico, G. E.; Schwartz, R. L.; Casey, S. M.; Lineberger, W. C. Naphthyl radical: negative ion photoelectron spectroscopy, Franck-Condon simulation, and thermochemistry. *J. Phys. Chem. A* **2001**, *105*, 10822−10381.
(73) Genossar, N.; Changala, P. B.; Gans, B.; Loison, J.-C.; Hartweg, S.; Martin-Drumel, M.-A.; Garcia, G. A.; Stanton, J. F.; Ruscic, B.; Baraban, J. H. Ring-opening dynamics of the cyclopropyl radical and cation: the transition state nature of the cyclopropyl cation. *J. Am. Chem. Soc.* **2022**, *144*, 18518−18525.

https://doi.org/10.1021/acs.jpclett.3c01243
J. Phys. Chem. Lett. 2023, 14, 5370−5376